Fracture analysis in 2D plane strain problems for composite materials containing hard inclusions and voids using an extended consecutive-interpolation quadrilateral element

Binh Hai Hoang[1, 2], Vay Siu Lo[1, 2], Bang Kim Tran[1, 2], Thien Tich Truong[1, 2, *]

[1]*Department of Engineering Mechanics, Faculty of Applied Science, Ho Chi Minh City University of Technology (HCMUT), 268 Ly Thuong Kiet Street, District 10, Ho Chi Minh City, Viet Nam*
[2]*Vietnam National University Ho Chi Minh City, Linh Trung Ward, Thu Duc City, Ho Chi Minh City, Viet Nam*

[*]Email: *tttruong@hcmut.edu.vn*

Abstract. This paper investigates fracture mechanics in particle-reinforced composites by using the extended finite element method enhanced by the consecutive-interpolation quadrilateral element. These composite materials have discontinuous boundaries such as cracks, voids and hard inclusions. The extended consecutive-interpolation quadrilateral element (XCQ4) is employed to model these boundaries in two-dimensional linear elastic deformation problems. XCQ4 combines the enrichment functions in the traditional extended finite element method with the consecutive interpolation on a 4-node quadrilateral element. This element uses both nodal values and averaged nodal gradients as interpolated conditions. In fracture analysis, the stress intensity factors (SIFs) are important parameters that must be defined. In this study, the values of SIFs at the crack tips are evaluated with the help of the interaction integrals approach. The critical angle for crack growth direction is based on the maximum circumferential tensile stress criterion. The obtained numerical results are compared with other reliable results showing high accuracy and convergence rate of the XCQ4 element.

1. INTRODUCTION

Particle-reinforced composites are materials that combine hard particles with other matrix materials. They have better mechanical properties than traditional materials. In the fracture analysis of cracks in particle-reinforced composites, there are discontinuous interface material boundaries and the presence of defects such as cracks, voids, and holes. These boundaries are hard to simulate with the conventional finite element method since it needs a lot of meshing

effort and requires high computational costs. Therefore, an extended algorithm has been developed to address crack-related issues.

The extended finite element method (XFEM) was first introduced in [1, 2]. The improved XFEM in the fact that the discontinuity and singularity induced by the crack are effectively treated as the mesh is completely independent of the crack geometry, and more interestingly the re-meshing in crack propagation is no longer required. XFEM method does not attempt to directly model cracks as geometric discontinuities. Instead, mathematical functions namely enrichments based on the partition of unity principle are used to capture the effect of displacement jump across crack surfaces and stress singularity in the vicinity of the crack tip. The method is then widely used in fracture analysis [3 - 5].

Since the conventional 4-node quadrilateral element can produce the discontinuous nodal gradient, Bui *et al.* [6] have succeeded in establishing a consecutive-interpolation 4-node quadrilateral element (CQ4), based on the idea of [7, 8]. The basic functions of CQ4 are built with the twice-interpolation procedure to obtain functions of continuous form and have higher-order polynomials without increasing the total number of degrees of freedom. The stress field becomes continuous without complicated treatment, the calculation results have significantly increased convergence compared with the traditional finite element method. This consecutive-interpolation concept is then applied in the 3D solid structure analysis [9 - 11].

For simulating fracture problems, the concept of XFEM has been incorporated into a consecutive-interpolation procedure to form the XCQ4 element [12 - 14]. The method is then used for analyzing crack in homogeneous plates [15], crack on the interface of bimaterial plates [16] and cracked functionally graded material (FGM) plates [17]. Compared with the standard extended 4-node quadrilateral element (XQ4), the new XCQ4 is primarily distinguished by the employment of nodal gradients into interpolation due to the consecutive-interpolation procedure (CIP). The approximation functions for the consecutive-interpolation quadrilateral element are extended to involve known enrichment functions.

This paper investigates the fracture behavior and the crack growth of cracked plates with discontinuous interfaces such as inclusions and voids by using the XCQ4 element. Cracked plates including hard inclusions and voids are already studied by the traditional XFEM in [18] but are not examined in the XCQ4 approach so far. And due to the authors' best knowledge, the crack propagation in the cracked plate with the combination of multiple inclusions and voids has not been reported, even by using the traditional XFEM. This is an important type of problem that needs attention because it involves investigating the mechanical properties of particle-reinforced composite structures. The accuracy and performance of the XCQ4 element are demonstrated through many numerical examples of 2D plane strain problems. The obtained results are compared with available numerical results showing good agreement. Moreover, the examples also show that the mechanical behavior becomes better when mixing hard particles compared with homogeneous material.

2. METHODOLOGY

2.1. The consecutive-interpolation 4-node quadrilateral element (CQ4)

To begin with the concept of consecutive-interpolation procedure, let an arbitrary point $\mathbf{x} = (x, y)$ located inside a four-node (i, j, k and m) quadrilateral element (see Figure 1). Denoting S_i, S_j, S_k and S_m, in that order, are neighbor elements that share the same node i, j, k and m. The

supporting nodes for the point **x** in this CQ4 element involve all nodes of S_i, S_j, S_k and S_m elements.

The approximation equation at point **x** is written as

$$\hat{u}(x) = \sum_{l=1}^{n_s} \hat{N}_l(x) u_l = \hat{\mathbf{N}}(\mathbf{x})\mathbf{u} \tag{1}$$

In equation 1, the consecutive-interpolation shape function $\hat{N}_l$ is determined by [12]

$$\hat{N}_l = \underbrace{\phi_i N_l^{[i]} + \phi_{ix} \bar{N}_{l,x}^{[i]} + \phi_{iy} \bar{N}_{l,y}^{[i]}}_{node\ i} + \underbrace{\phi_j N_l^{[j]} + \phi_{jx} \bar{N}_{l,x}^{[j]} + \phi_{jy} \bar{N}_{l,y}^{[j]}}_{node\ j}$$
$$+ \underbrace{\phi_k N_l^{[k]} + \phi_{kx} \bar{N}_{l,x}^{[k]} + \phi_{ky} \bar{N}_{l,y}^{[k]}}_{node\ k} + \underbrace{\phi_m N_l^{[m]} + \phi_{mx} \bar{N}_{l,x}^{[m]} + \phi_{my} \bar{N}_{l,y}^{[m]}}_{node\ m} \tag{2}$$

in which $N_l^{[i]}$ is the shape function with respect to node i, and n_s is the total number of the supporting nodes in regard to the point **x**.
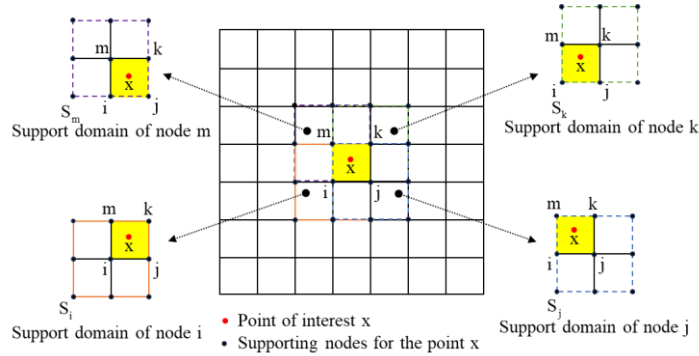

Figure 1. Illustration of CQ4 element and its supporting node in 2-D domain.

According to [12] and [13], the formulation of the average derivative of the shape functions at node i is given as the following expression

$$\bar{N}_{l,x}^{[i]} = \sum_{e \in s_i} \left(\omega_e N_{l,x}^{[i][e]} \right); \quad \bar{N}_{l,y}^{[i]} = \sum_{e \in s_i} \left(\omega_e N_{l,y}^{[i][e]} \right) \tag{3}$$

where the term $N_{l,x}^{[i][e]}$ is the derivative computed in element e, and ω_e is the weight function of element $e \in S_i$, which is defined as

$$\omega_e = \frac{\Delta_e}{\sum_{e' \in S_i} \Delta_{e'}} \tag{4}$$

in which Δ_e is area of the element e.

In equation 2, the functions ϕ_i, ϕ_{ix}, and ϕ_{iy} forming the polynomial basis associated with node i must satisfy the following conditions:

$$\begin{aligned}
\phi_i(\mathbf{x}_l) &= \delta_{il}, & \phi_{i,x}(\mathbf{x}_l) &= 0, & \phi_{i,y}(\mathbf{x}_l) &= 0 \\
\phi_{ix}(\mathbf{x}_l) &= 0, & \phi_{ix,x}(\mathbf{x}_l) &= \delta_{il}, & \phi_{ix,y}(\mathbf{x}_l) &= 0 \\
\phi_{iy}(\mathbf{x}_l) &= 0, & \phi_{iy,x}(\mathbf{x}_l) &= 0, & \phi_{iy,y}(\mathbf{x}_l) &= \delta_{il}
\end{aligned} \tag{5}$$

where l is any one of the indices i, j, k, and m, and

$$\delta_{il} = \begin{cases} 1, & \text{if } i = l \\ 0, & \text{if } i \neq l \end{cases} \tag{6}$$

The polynomial basis functions $\phi_i, \phi_{ix}, \phi_{iy}$ for the quadrilateral element are given as

$$\phi_i = N_i + N_i^2 N_j + N_i^2 N_k + N_i^2 N_m - N_i N_j^2 - N_i N_k^2 - N_i N_m^2 \tag{7}$$

$$\begin{aligned}
\phi_{ix} = &-(x_i - x_j)(N_i^2 N_j + bN_i N_j N_k + bN_i N_j N_m) \\
&-(x_i - x_k)(N_i^2 N_k + bN_i N_k N_m + bN_i N_k N_j) \\
&-(x_i - x_m)(N_i^2 N_m + bN_i N_m N_j + bN_i N_m N_k)
\end{aligned} \tag{8}$$

$$\begin{aligned}
\phi_{iy} = &-(y_i - y_j)(N_i^2 N_j + bN_i N_j N_k + bN_i N_j N_m) \\
&-(y_i - y_k)(N_i^2 N_k + bN_i N_k N_m + bN_i N_k N_j) \\
&-(y_i - y_m)(N_i^2 N_m + bN_i N_m N_j + bN_i N_m N_k)
\end{aligned} \tag{9}$$

with $b = 1/2$ and the functions $\phi_j, \phi_{jx}, \phi_{jy}, \phi_k, \phi_{kx}, \phi_{ky}, \phi_m, \phi_{mx}$, and ϕ_{my} can be also calculated in the same manner by a circulatory permutation of indices *i, j, k,* and *m*. In addition, N_i, N_j, N_k and N_m are the Lagrange basis function.

2.2. The extended consecutive-interpolation 4-node quadrilateral element (XCQ4)

Figure 2 shows the typical discontinuities often occur in particle composite. Based on the XFEM approach, the XCQ4 approximation of the displacement field is written as follows

$$\mathbf{u}^h(\mathbf{x}) = \hat{\mathbf{u}}(\mathbf{x}) + \hat{\mathbf{u}}^{enr}(\mathbf{x}) = \sum_{j=1}^{n_s} \hat{N}_j(\mathbf{x}) u_j + \sum_{l=1}^{np} \sum_{k=1}^{m} \hat{N}_k(\mathbf{x}) \hat{\psi}^l(\mathbf{x}) a_k^l \tag{10}$$

where the first term on the right-hand side is the familiar approximation by CQ4 (see equation 1), *np* is the number of discontinuous conditions (crack, inclusion, void) that occur for an element containing **x**, *m* is the number of enriched nodes in each *np*, $\hat{\psi}$ is the enrichment function in each condition *np*.
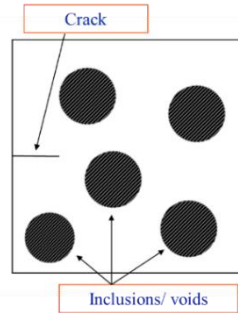

Figure 2. Discontinuous boundaries in a particle composite material includes defects such as cracks, voids, and hard inclusions.

The discrete system of linear equilibrium equation under small strain condition can be expressed as

$$\mathbf{K}\mathbf{u}^h = \mathbf{F} \tag{11}$$

where $\mathbf{u}^h$ contains the normal displacements **u** and the enriched degrees of freedom **a**

$$\mathbf{u}^h = \{\mathbf{u}, \mathbf{a}\}^T \tag{12}$$

K is the global stiffness matrix and **F** is the external load vector, for enriched elements, the elementary stiffness matrix is obtained as

$$\mathbf{K}_{ij}^e = \begin{bmatrix} \mathbf{K}_{ij}^{\mathbf{uu}} & \mathbf{K}_{ij}^{\mathbf{ua}} \\ \mathbf{K}_{ij}^{\mathbf{au}} & \mathbf{K}_{ij}^{\mathbf{aa}} \end{bmatrix}; \quad \mathbf{F}_i^{\mathbf{u}} = \mathbf{F}_i^e \tag{13}$$

in which $\mathbf{K}_{ij}^{\mathbf{uu}}$, $\mathbf{K}_{ij}^{\mathbf{ua}}$, $\mathbf{K}_{ij}^{\mathbf{au}}$, and $\mathbf{K}_{ij}^{\mathbf{aa}}$ are defined as

$$\mathbf{K}_{ij}^{rs} = \int_\Omega \left(\mathbf{B}_i^r\right) \mathbf{D}\mathbf{B}_j^s d\Omega \qquad r,s = \mathbf{u}, \mathbf{a} \tag{14}$$

The **B**-operator is the matrix of the derivatives of shape functions and is expressed as

$$\mathbf{B}_i^{\mathbf{u}} = \begin{bmatrix} \hat{N}_{i,x} & 0 \\ 0 & \hat{N}_{i,y} \\ \hat{N}_{i,y} & \hat{N}_{i,x} \end{bmatrix}; \quad \mathbf{B}_i^{\mathbf{a}} = \begin{bmatrix} \hat{\psi}(\mathbf{x})\hat{N}_{i,x} + \hat{\psi}(\mathbf{x})_{,x}\hat{N}_i & 0 \\ 0 & \hat{\psi}(\mathbf{x})\hat{N}_{i,y} + \hat{\psi}(\mathbf{x})_{,y}\hat{N}_i \\ \hat{\psi}(\mathbf{x})\hat{N}_{i,y} + \hat{\psi}(\mathbf{x})_{,y}\hat{N}_i & \hat{\psi}(\mathbf{x})\hat{N}_{i,x} + \hat{\psi}(\mathbf{x})_{,x}\hat{N}_i \end{bmatrix} \tag{15}$$

and **D** is the material matrix, for the plane strain state

$$\mathbf{D} = \frac{E}{(1+v)(1-2v)} \begin{bmatrix} 1-v & v & 0 \\ v & 1-v & 0 \\ 0 & 0 & (1-2v)/2 \end{bmatrix} \tag{16}$$

The enrichment functions $\hat{\psi}(\mathbf{x})$ of the XCQ4 for cracks, hard inclusions, and voids in the composite material are shown below.
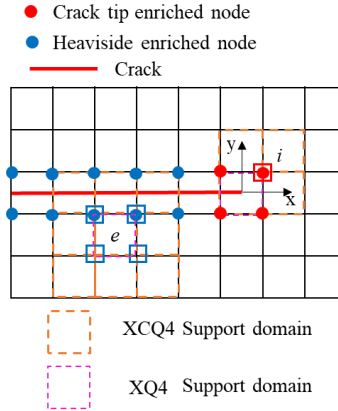
2.2.1. XCQ4 approximation for cracks

Figure 3. Support domains of XCQ4 and XQ4, and their enriched nodes.

The support domains of a Heaviside enriched node for a continuous element *e* and a crack-tip enriched node *i* are schematically shown in Figure 3. It can be recognized that the support domain with respect to an enriched node would result in the continuity of the nodal derivatives [7]. However, due to the discontinuity, the C^0-continuity at nodes is expected. One alternative option is to improve the computation of the average nodal gradient for enriched nodes as [8]

$$\bar{N}_{f,x}^{[i]} = N_{f,x}^{[i][e]} \, , \bar{N}_{f,y}^{[i]} = N_{f,y}^{[i][e]} \tag{17}$$

For the split nodes, enrichment functions $\hat{\psi}(\mathbf{x})$ is the Heaviside function $H(\mathbf{x})$. The Heaviside function is used in elements which have their support completely cut by the crack [15]

$$H(\mathbf{x}) = \begin{cases} 1, & \text{for } f(\mathbf{x}) > 0 \\ -1, & \text{for } f(\mathbf{x}) < 0 \end{cases} \tag{18}$$

$f(\mathbf{x})$ is the sign distance function.

Now the matrix $\mathbf{B}^a$ for the split nodes (in Eq. (15)) has the following form

$$\mathbf{B}_i^{spl} = \begin{bmatrix} \left(\hat{N}_i\left[H(\mathbf{x}) - H(\mathbf{x}_i)\right]\right)_{,x} & 0 \\ 0 & \left(\hat{N}_i\left[H(\mathbf{x}) - H(\mathbf{x}_i)\right]\right)_{,y} \\ \left(\hat{N}_i\left[H(\mathbf{x}) - H(\mathbf{x}_i)\right]\right)_{,y} & \left(\hat{N}_i\left[H(\mathbf{x}) - H(\mathbf{x}_i)\right]\right)_{,x} \end{bmatrix} \tag{19}$$

For the tip nodes, enrichment functions $\hat{\psi}(\mathbf{x})$ is the function $F_\alpha(\mathbf{x})$. Crack tip enrichment functions embed the crack tip singularity into the enriched element

$$\left\{F_\alpha(r,\theta)\right\}_{\alpha=1}^4 = \left\{\sqrt{r}\sin\frac{\theta}{2}, \sqrt{r}\cos\frac{\theta}{2}, \sqrt{r}\sin\frac{\theta}{2}\sqrt{r}\sin\theta, \sqrt{r}\cos\frac{\theta}{2}\sqrt{r}\sin\theta\right\} \tag{20}$$

The near crack tip enriched $\mathbf{B}^a$ matrix in equation 15 now has the form

$$\mathbf{B}_i^{tip\alpha} = \begin{bmatrix} \left(\hat{N}_i\left[F_\alpha(\mathbf{x}) - F_\alpha(\mathbf{x}_i)\right]\right)_{,x} & 0 \\ 0 & \left(\hat{N}_i\left[F_\alpha(\mathbf{x}) - F_\alpha(\mathbf{x}_i)\right]\right)_{,y} \\ \left(\hat{N}_i\left[F_\alpha(\mathbf{x}) - F_\alpha(\mathbf{x}_i)\right]\right)_{,y} & \left(\hat{N}_i\left[F_\alpha(\mathbf{x}) - F_\alpha(\mathbf{x}_i)\right]\right)_{,x} \end{bmatrix} \quad \alpha = 1,2,3,4 \tag{21}$$

$$\mathbf{B}_i^{tip} = \begin{bmatrix} \mathbf{B}_i^{tip1} & \mathbf{B}_i^{tip2} & \mathbf{B}_i^{tip3} & \mathbf{B}_i^{tip4} \end{bmatrix} \tag{22}$$

2.2.2. XCQ4 approximation for inclusions

As stated in the first section, this study aims to examine cracked plates with inclusions and voids inside. To model the discontinuity due to the appearance of hard inclusions in an extended concept, an appropriate enrichment function must be used. The enrichment function for inclusion [16, 19] is defined as follows

$$\chi(\mathbf{x}) = \sum_i \hat{N}_i(\mathbf{x})\left|f_i(\mathbf{x})\right| - \left|\sum_i \hat{N}_i(\mathbf{x})\, f_i(\mathbf{x})\right| \tag{23}$$

where $f_i(\mathbf{x})$ is distance function of node i can be defined as

$$f(\mathbf{x}) = \left\|\mathbf{x} - \mathbf{x}_c\right\| - r_c \tag{24}$$

in which x_c and r_c are center and radius of the inclusion.

The entries of the $\mathbf{B}^a$ matrix for inclusions

$$\mathbf{B}_i^{inc} = \begin{bmatrix} \hat{N}_{i,x}\chi(\mathbf{x}_i) + \hat{N}_i\chi(\mathbf{x}_i)_{,x} & 0 \\ 0 & \hat{N}_{i,y}\chi(\mathbf{x}_i) + \hat{N}_i\chi(\mathbf{x}_i)_{,y} \\ \hat{N}_{i,y}\chi(\mathbf{x}_i) + \hat{N}_i\chi(\mathbf{x}_i)_{,y} & \hat{N}_{i,x}\chi(\mathbf{x}_i) + \hat{N}_i\chi(\mathbf{x}_i)_{,x} \end{bmatrix} \tag{25}$$

where the derivative of $\chi(\mathbf{x})$ with respect to x and y are computed as

$$\chi(\mathbf{x})_{,x} = \sum_i \frac{\partial \hat{N}_i(\mathbf{x})}{\partial x}|f_i(\mathbf{x})| - \frac{\sum_i \hat{N}_i(\mathbf{x}) f_i(\mathbf{x})}{\left|\sum_i \hat{N}_i(\mathbf{x}) f_i(\mathbf{x})\right|} \sum_i \frac{\partial \hat{N}_i(\mathbf{x})}{\partial x} f_i(\mathbf{x})$$

$$\chi(\mathbf{x})_{,y} = \sum_i \frac{\partial \hat{N}_i(\mathbf{x})}{\partial y}|f_i(\mathbf{x})| - \frac{\sum_i \hat{N}_i(\mathbf{x}) f_i(\mathbf{x})}{\left|\sum_i \hat{N}_i(\mathbf{x}) f_i(\mathbf{x})\right|} \sum_i \frac{\partial \hat{N}_i(\mathbf{x})}{\partial y} f_i(\mathbf{x})$$

(26)

2.2.3. XCQ4 approximation for voids

Besides inclusion, void is also a feature that the study concerns. According to [20, 21] void enrichment function is used in elements which contain void boundary

$$V(\mathbf{x}) = \begin{cases} 1, & if \; f(\mathbf{x}) > 0 \\ 0, & if \; f(\mathbf{x}) < 0 \end{cases} \tag{27}$$

Now the matrix $\mathbf{B}^a$ for voids has the following form

$$\mathbf{B}_i^{hole} = \begin{bmatrix} \hat{N}_{i,x}\left[V(\mathbf{x}) - V(\mathbf{x}_i)\right] & 0 \\ 0 & \hat{N}_{i,y}\left[V(\mathbf{x}) - V(\mathbf{x}_i)\right] \\ \hat{N}_{i,y}\left[V(\mathbf{x}) - V(\mathbf{x}_i)\right] & \hat{N}_{i,x}\left[V(\mathbf{x}) - V(\mathbf{x}_i)\right] \end{bmatrix} \tag{28}$$

2.4. Stress intensity factors calculation

In the interaction integral approach, two states of a cracked body are considered: the actual state #1 ($\sigma_{ij}^{(1)}, \varepsilon_{ij}^{(1)}, u_i^{(1)}$) and the auxiliary state #2 ($\sigma_{ij}^{(2)}, \varepsilon_{ij}^{(2)}, u_i^{(2)}$). The relation between the interaction integral and the mixed-mode stress intensity factors (SIFs) is as follows

$$M^{(1+2)} = \frac{2}{E^*}\left(K_I^{(1)}K_I^{(2)} + K_{II}^{(1)}K_{II}^{(2)}\right) \tag{29}$$

where $E^* = \dfrac{E}{1-\nu^2}$ is the effective Young's modulus for the plane strain state.

M is the interaction integral, which can be computed as

$$M^{(1+2)} = \int_A \left[-W^{(1,2)}\delta_{1j} + \sigma_{ij}^{(1)}\frac{\partial u_i^{(2)}}{\partial x_j} + \sigma_{ij}^{(2)}\frac{\partial u_i^{(1)}}{\partial x_j}\right]\frac{\partial q}{\partial x_j}dA \tag{30}$$

in which $q(\mathbf{x})$ is the weight function which has the value of 1 on the open set containing the crack tip and 0 on the outer prescribed contour (the red curve in Figure 4).

By choosing $K_I^{(2)} = 1$, $K_{II}^{(2)} = 0$ for mode I and $K_I^{(2)} = 0$, $K_{II}^{(2)} = 1$ for mode II, the corresponding SIFs are obtained

$$K_I^{(1)} = \frac{E^*}{2} M^{(1,ModeI)}; \quad K_{II}^{(1)} = \frac{E^*}{2} M^{(1,ModeII)} \tag{31}$$

It is noted that by incorporating CIP into the approximation, the support domain for the element belonging to *J*-domain in terms of the XCQ4 (denoted by the blue dash line) is larger than that of the standard XQ4.
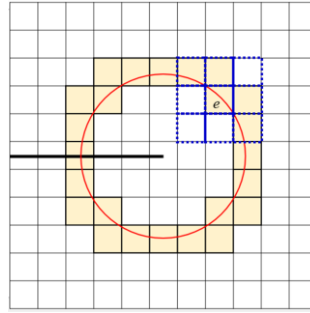

Figure 4. J-integral domain in XCQ4.
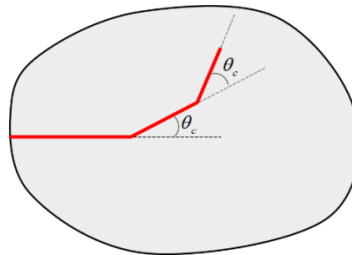
2.5. Crack growth simulation

Figure 5. Critical angle in crack growth simulation.

To model crack growth in this paper, the maximum circumferential tensile stress criterion is adopted. The critical angle θ_c (see Figure 5) of the propagation direction is defined from the SIFs of the mixed-mode problem [22]

$$\theta_c = 2\arctan\left(\frac{1 - \sqrt{1 + 8\left(K_{II}/K_I\right)^2}}{4\left(K_{II}/K_I\right)}\right) \tag{32}$$

The procedure to simulate crack propagation in the XCQ4 approach is similar to the procedure of the traditional XFEM and can be found in [23].

3. RESULTS AND DISCUSSIONS

3.1. A rectangular plate containing an edge crack

A rectangular plate containing an edge crack is considered for the validation study (see Figure 6). The dimension of the rectangular plate is 72 mm × 36 mm. The plate is fixed on the bottom

edge and subjected to tensile stress $\sigma = 1.1$ N/mm^2 on the top edge [24]. Various crack lengths are considered with the ratios $a/W = 0.3$, 0.4, 0.5 and 0.6. The material properties of polycarbonate are given as: $E = 2.50$ GPa and $\nu = 0.38$.

(a)   (b)   (c)
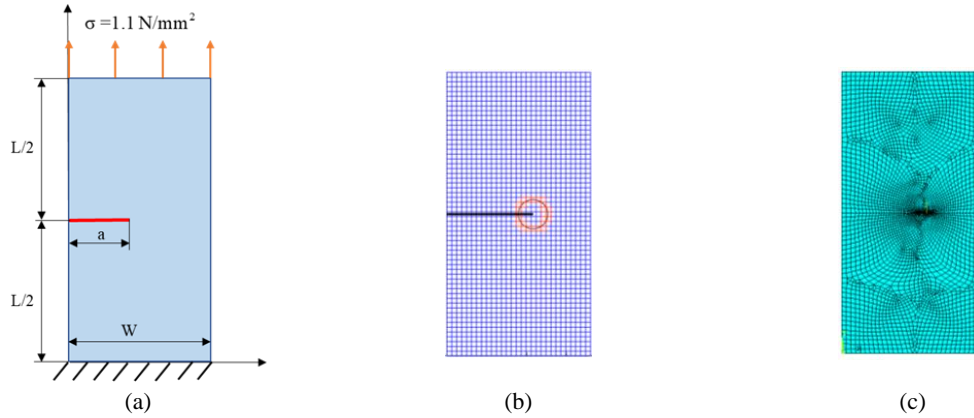
Figure 6. Rectangular plate containing an edge crack: (a) Geometry, boundary conditions and loadings, (b) The mesh used in XCQ4 and XFEM, (c) The mesh used in FEM.

Firstly, the obtained results from XCQ4 are compared with XQ4 and the analytical solution [25]. The analytical results of K_I can be calculated as

$$K_I = \left[1.12 - 0.231\left(\frac{a}{W}\right) + 10.55\left(\frac{a}{W}\right)^2 - 21.72\left(\frac{a}{W}\right)^3 + 30.39\left(\frac{a}{W}\right)^4 \right] \sigma \sqrt{\pi a} \qquad (32)$$

Table 1. The values of K_I in different methods and mesh sizes.

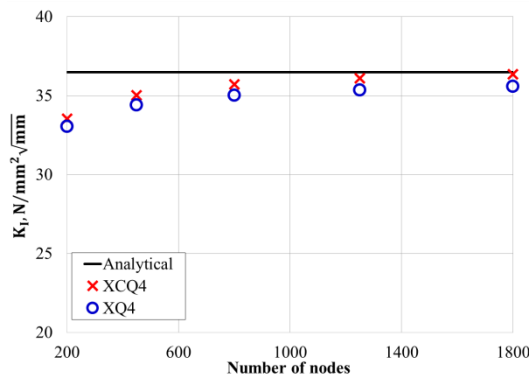| Method	10×20	15×30	20×40	25×50	30×60
Analytical [25]	36.4850	36.4850	36.4850	36.4850	36.4850
XQ4	33.0533	34.4073	35.0227	35.3687	35.5886
XCQ4	33.5438	35.0235	35.7183	36.1154	36.3718

Figure 7. Convergence of K_I with respect to the number of nodes.

The a/W ratio is assumed to be 0.6 in this case. The values of K_I computed with various meshing models using both XCQ4 and XQ4 approaches are provided in Table 1, together with

the analytical solution. Figure 7 further demonstrates the convergence of K_I evaluated by XCQ4 and XQ4 elements with respect to number of nodes. The numerical results of mode-I SIF quickly approach the analytical solution. However, it can be seen that the XCQ4 has higher accuracy than the conventional XQ4.

The distribution of normal stress component σ_y obtained by both XCQ4 and XQ4 elements is shown in Figure 8. It can be seen that by using XCQ4, the stress σ_y varies smoothly across element edges, while that by XQ4 is non-physically discontinuous. Therefore, the XCQ4 element is better in the context of providing a smoother stress field.
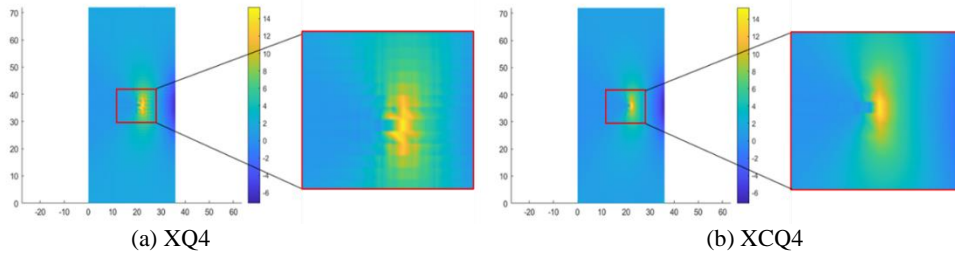

(a) XQ4   (b) XCQ4

Figure 8. Comparison of stress distribution σ_y (unit: N/mm^2) between (**a**) XQ4 and (**b**) XCQ4.

Now consider the variation of K_I when the crack length varies. A 30×60 mesh is used for both XCQ4 and XQ4 approaches (Figure 6 (b)). The mesh of the finite element model is adaptive with different crack lengths (Figure 6 (c)), so the total number of nodes is not fixed but ranges from 11513 to 12059 nodes (the Plane183 element is used). The FEM model from now on is conducted by using the ANSYS commercial software. The ANSYS set-up is calibrated in this example for use in subsequent problems.

Table 2. Values of K_I in different a/W ratios and methods.

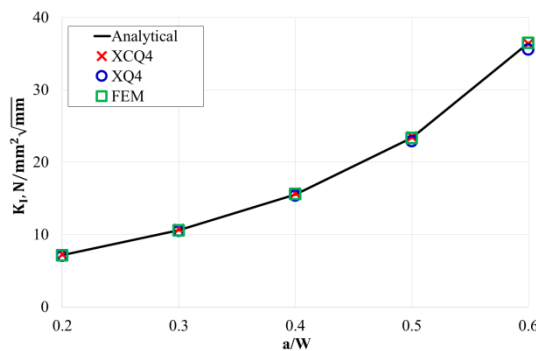| Method	$a/W = 0.2$	0.3	0.4	0.5	0.6
Analytical [25]	7.1708	10.6357	15.5630	23.3794	36.4850
FEM	7.1067	10.5870	15.6070	23.3460	36.4780
XQ4	7.0753	10.5032	15.3786	22.8981	35.5886
XCQ4	7.2684	10.7819	15.7709	23.5246	36.3718

Figure 9. Variation of K_I with respect to a/W for an edge crack plate under tensile loading.

Table 2 and Figure 9 show the variation of K_I with respect to the a/W ratio in different methods. From the figure one can notice that K_I tends to increase as the crack length increases. Furthermore, XCQ4 is observed to be in good agreement with analytical solutions, extended finite element method and the conventional finite element method.

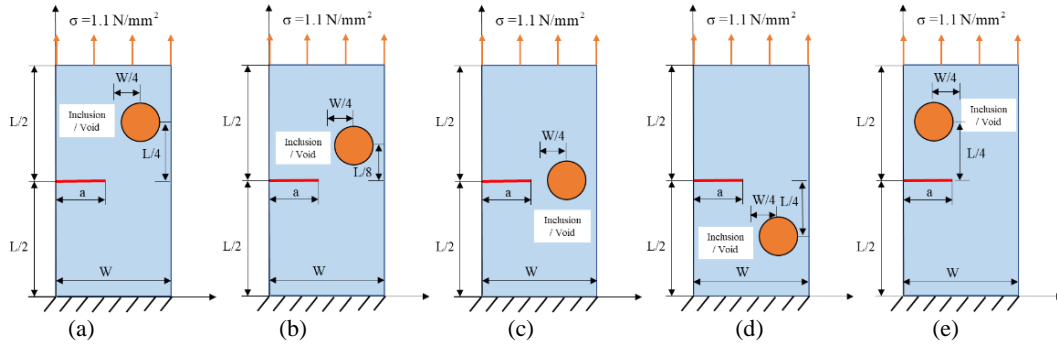### 3.2. A rectangular plate containing an edge crack and a single inclusion/void

Figure 10. An edge crack plate with a single inclusion/void under tensile loading.

Figure 10 (a)-(e) shows the geometry of a rectangular plate containing an edge crack and a single inclusion/void. The plate is subjected to a uniform distributed load $\sigma = 1.1$ N/mm² on the top edge and the bottom edge is fixed. The geometry dimensions are: 72 mm × 36 mm, various crack length ratios are considered $a/W = 0.2$, 0.3, 0.4 and 0.5. The radius of the circular hard inclusion is 6 mm, and the position of the hard inclusion is shown in Figure 10 (a)-(e). The material properties of polycarbonate are given as: $E = 2.50$ GPa and $\nu = 0.38$. The hard inclusion is made of AZ61 with the ratio $E_{inclusion}/E = 18$. For the XCQ4 and XQ4 models, the plate is discretized into 30×60 nodes, and for the FEM model used in ANSYS, the total number of nodes is not fixed but ranges from 7589 to 10063 nodes (the Plane183 element is used).

Table 3. The values of K_I in different a/W ratios and methods. The case of a single hard inclusion.

Model	Method	$a/W = 0.2$	0.3	0.4	0.5
Figure 10 (a)	XCQ4	7.2388	10.6697	15.7944	23.5950
	XQ4	6.8809	10.1279	14.7602	22.0228
	FEM	7.0068	10.3530	15.1680	22.7620
Figure 10 (b)	XCQ4	7.3740	10.6175	15.2286	21.8592
	XQ4	7.0035	10.0673	14.2187	20.3904
	FEM	7.1310	10.2620	14.6040	21.0410
Figure 10 (c)	XCQ4	7.6263	10.9425	15.4913	20.4670
	XQ4	7.2428	10.3724	14.4426	19.5411
	FEM	7.3770	10.6250	14.8250	19.4980
Figure 10 (d)	XCQ4	7.2446	10.6758	15.7998	23.5979
	XQ4	6.8809	10.1278	14.7599	22.0219
	FEM	6.9987	10.3400	15.1430	22.7280
Figure 10 (e)	XCQ4	7.0325	10.7446	16.1860	24.2050
	XQ4	6.6966	10.2002	15.1129	22.5693
	FEM	6.8104	10.3950	15.4990	23.3390

The results of mode-I SIF calculation are presented in Table 3. Similar to the first example, K_I tends to increase as the a/W ratio increases. Compared to the results of the previous example, it is shown that the stress intensity factor is significantly improved when a homogeneous plate material is reinforced with hard inclusion. For example, in the case of $a/W = 0.5$ and the position of the inclusion is as in Figure 10 (c), mode-I SIF decreases by approximately 12%.

In the second case, the void is considered instead of the inclusion. The geometry is illustrated in Figure 10, a circular void of radius $R = 6$ mm replaces the circular hard inclusion. The meshes for XCQ4, XQ4 and ANSYS are set up the same as the first case. The results of mode-I SIF calculation are presented in Table 4. Although the hard inclusion is replaced by the void, K_I still increases as the a/W ratio increases. In contrast to the reinforced material with hard inclusions, the mode-I SIF significantly increases when a void appears. For example, at the crack tip located near the hole (Figure 10 (c) and $a/W=0.5$), the stress intensity factor increase by up to 30% compared to the homogeneous material.

Table 4. The values of K_I in different a/W ratios and methods. The case of a single void.

Model	Method	$a/W = 0.2$	0.3	0.4	0.5
Figure 10 (a)	XCQ4	7.4635	11.4452	17.3346	25.8259
	XQ4	7.0993	10.8535	16.1621	24.0358
	FEM	7.2328	11.1360	16.7080	25.0160
Figure 10 (b)	XCQ4	7.0538	11.4693	18.6905	30.7334
	XQ4	6.7151	10.8974	17.4691	28.6780
	FEM	6.8238	11.1360	18.0840	30.1130
Figure 10 (c)	XCQ4	6.3747	10.4669	17.2571	31.3872
	XQ4	6.0696	9.9490	16.1611	29.1860
	FEM	6.1393	10.1600	16.5910	30.8450
Figure 10 (d)	XCQ4	7.4512	11.4032	17.2619	25.7456
	XQ4	7.1108	10.8451	16.1325	23.9991
	FEM	7.2066	11.0710	16.5990	24.8880
Figure 10 (e)	XCQ4	8.1038	11.3110	16.2953	24.1237
	XQ4	7.6661	10.7208	15.2289	22.5092
	FEM	7.8747	10.9680	15.6280	23.2720

3.3. A rectangular plate containing an edge crack and mixing inclusions and voids
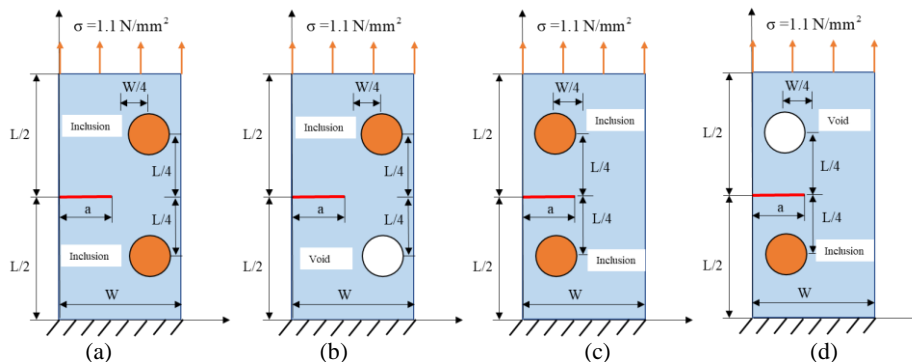

Figure 11. An edge crack plate with a single inclusion/void under tensile loading.

This example examines a more complex problem where cracks, hard inclusion, and void are included. A rectangular plate containing an edge crack and mixing single hard inclusion and single void under tensile loading is shown in Figure 11. The plate dimension is 72 mm × 36 mm, various crack length ratio a/W is considered. Material properties of the plate and inclusions are considered the same as the previous example. The position of void and inclusion is shown in Figure 11. For the XCQ4 and XQ4 models, the plate is discretized into 30×60 nodes, and for the FEM model used in ANSYS, the total number of nodes is around 8500 nodes (the Plane183 element is used).

Mode I- SIFs are determined by XCQ4 for various crack length ratios a/W as shown in Table 5. It is observed from the table that K_I increases by increasing crack length ratio (a/W) for all four cases under tensile loading, maximum K_I is found in the mixing void and hard inclusion (case (b)); and minimum in two hard inclusions (case (a)). In addition, in the case where void and inclusion are on the right side of the plate (case (a)) when replacing inclusion with void (case (b)), the SIF changes significantly. While void and inclusion are on the left side of the plate (case (c) and (d)), this change is very small. This may be because the position of the void in case (b) (bottom) and in case (d) (top) is different.

Table 5. The values of K_I in different a/W ratios. The case of mixing inclusion and void.

Model	Method	a/W=0.2	0.3	0.4	0.5	0.6
Figure 11 (a)	XCQ4	7.1330	10.4211	15.3572	22.9995	36.3425
	XQ4	6.7764	9.8923	14.3597	21.4845	33.9809
	FEM	6.8905	10.0920	14.7130	22.1390	35.2170
Figure 11 (b)	XCQ4	7.3640	11.1746	16.8367	25.1457	38.6504
	XQ4	7.0282	10.6321	15.7459	23.4585	36.0711
	FEM	7.1222	10.8480	16.1840	24.2950	37.5710
Figure 11 (c)	XCQ4	6.72784	10.5823	16.1493	24.2227	37.6082
	XQ4	6.4143	10.0461	15.0720	22.5795	35.1063
	FEM	6.5063	10.2190	15.4290	23.3100	36.4890
Figure 11 (d)	XCQ4	7.7921	11.1396	16.2552	24.1407	37.5201
	XQ4	7.3776	10.5585	15.1848	22.5189	35.0333
	FEM	7.5618	10.7840	15.5560	23.2430	36.4070

3.4. A rectangular plate containing an edge crack and mixing two inclusions and two voids

In this example, a rectangular plate containing an edge crack with two inclusions and two voids is investigated (see Figure 12 (a)). The plate dimension is 72 mm × 36 mm. Material properties of the plate and inclusions are considered the same as the previous problems. The position of voids and inclusions is shown in Figure 12 (a). For the XCQ4 and XQ4 models, the plate is discretized into 30×60 nodes, and for the FEM model used in ANSYS, the total number of nodes is around 7600 nodes (the Plane183 element is used).

Table 6 shows the values of K_I determined by XCQ4 for various crack length ratios a/W. It is observed that K_I increase with the increase of the crack length ratio (a/W) for all cases under tensile loading. The obtained results are very good approximations to the results from the conventional finite element method and the extended finite element method.

Table 6. Values of K_I in different a/W ratios and methods.
The case of mixing two inclusions and two voids.

Method	$a/W = 0.2$	0.3	0.4	0.5	0.6
XCQ4	7.8505	11.4972	16.9938	25.1799	38.6132
XQ4	7.4695	10.9356	15.9054	23.5035	36.0456
FEM	7.5614	11.1170	16.2250	24.1140	37.2760

3.5. Crack growth in the plate with different loads and defects

In this final example, crack propagation problems are investigated. The plate dimension is 72 mm × 36 mm and the crack length $a = 10.8$ mm ($a/W = 0.3$). For the propagation simulation, the crack is assumed to grow in every step. 10 steps of propagation are simulated, the crack growth increment for each step $\Delta a = 2$ mm. The material properties of the plate and inclusions are identical to the previous problems. For the XCQ4 model, the plate is discretized into 30×60 nodes.

First, the position of the circular voids and hard circular inclusions is considered in Figure 12. The rectangular plate is fixed at the bottom edge. Three different load cases applied on the top edge are examined: tensile load, shear load and the combination of tensile and shear load. The magnitude of the uniform distributed load $\sigma = \tau = 1.1 \, N/mm^2$.
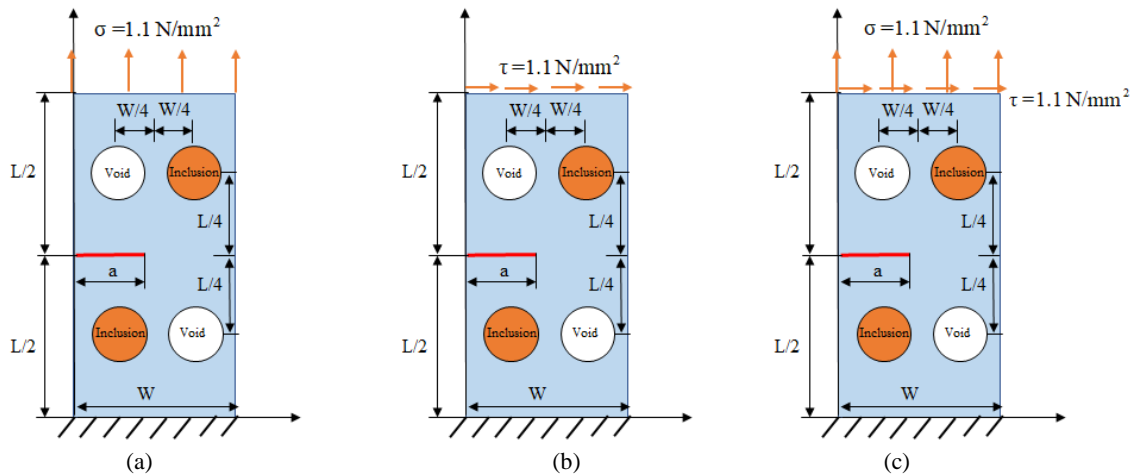

Figure 12. An edge crack plate with two inclusions and two voids. (a) tensile load, (b) shear load and (c) combination of tensile and shear loads.

Figure 13 shows the crack growth paths of three different load cases. In the figure, the magenta circle denotes the boundary of the hard inclusions while the black circle represents the boundary of the voids. The crack path in the case of the tensile load is a horizontal line (Figure 13 (a)), this is similar to the case of the homogeneous plate subjected to tensile load. In the two other cases, with the appearance of the shear load, the crack tends to propagate at an incline angle to the bottom edge. However, there is also a slight difference that can be observed in the two crack lines of cases (b) and (c).
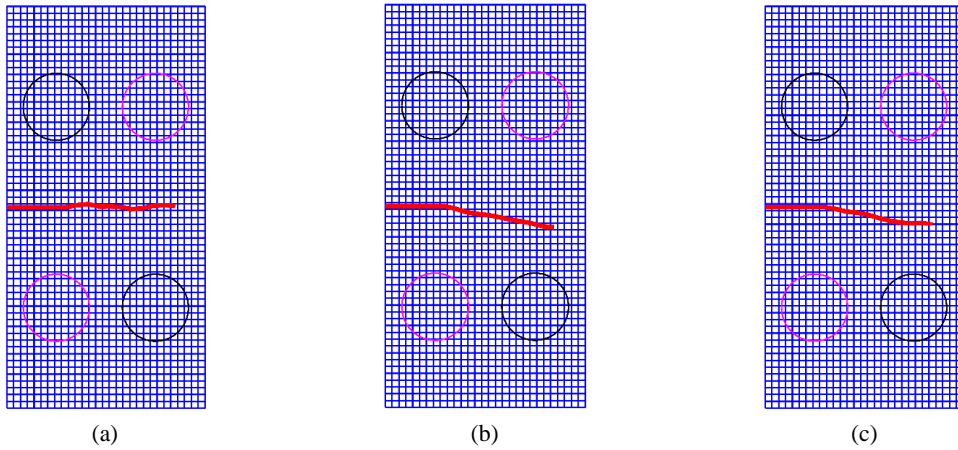
(a)   (b)   (c)

Figure 13. Crack growth paths of three different load cases. (a) tensile load, (b) shear load and
(c) combination of tensile and shear loads.

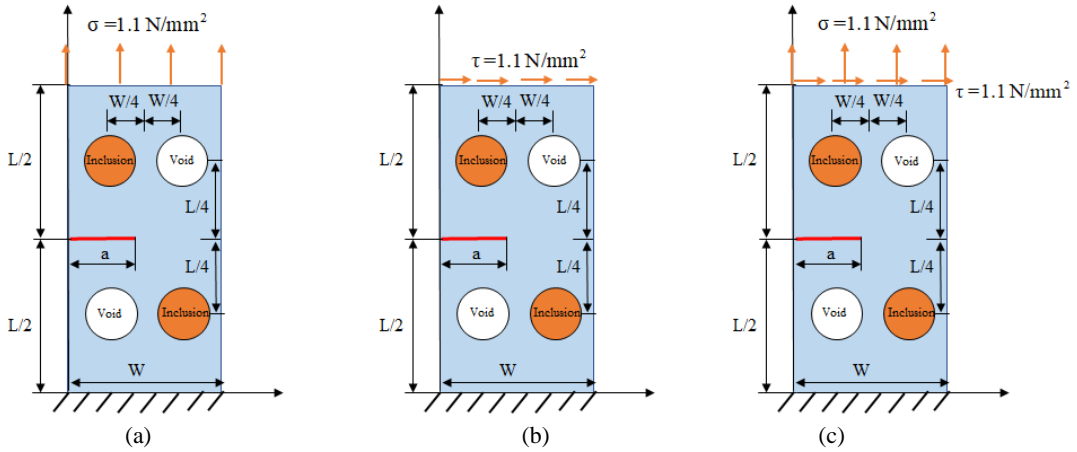(a)   (b)   (c)

Figure 14. An edge crack plate with different positions of inclusions and voids compared to Figure 14.
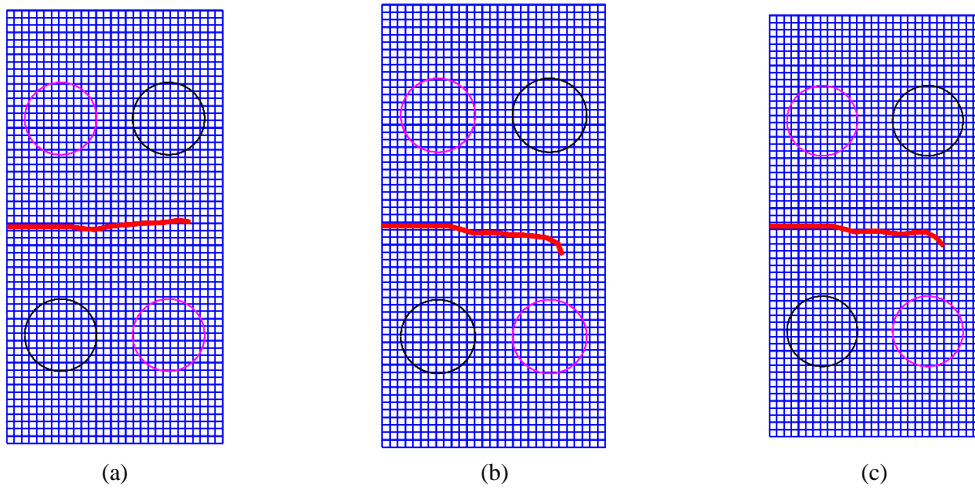(a) tensile load, (b) shear load and (c) combination of tensile and shear loads.

(a)   (b)   (c)

Figure 15. Crack growth paths of: (a) tensile load, (b) shear load and (c) combination of tensile and shear.

911

In the second case to be considered, the positions of the voids and the hard inclusions are interchanged so that the effect of the relative positions of the defects on the crack growth path can be observed. Similar to the first case, three different load cases are examined: tensile load, shear load and the combination of tensile and shear load (see Figure 14). The rectangular plate is also fixed at the bottom edge.

Figure 15 shows the crack growth paths of three different load cases. Different from Figure 13 (a), the crack path in Figure 15 (a) of the tensile load case is slightly upward toward the above circular hole. Meanwhile, in the remaining two cases, the influence of shear force is still strong enough to pull the crack path downward. However, the initial propagation angle is less inclined than the case in Figure 13 (b) and (c), but at the final propagation simulation step this inclined angle suddenly increases. In addition, the crack path in Figure 15 (b) is slightly more inclined than that in Figure 15 (c).

4. CONCLUSIONS

In this study, the XCQ4 is extended from the CQ4 element and combined with the enrichment functions to model discontinuous boundaries such as cracks, voids, and hard inclusions for the first time. Through many numerical examples, the SIF results obtained by XCQ4 agree well with the analytical and reference results. XCQ4 is shown to have a smoother stress field compared to XFEM due to the continuous gradient computation. With the inherent properties of XFEM, the XCQ4 element is convenient for those discontinuous boundaries without the need of conforming meshing these boundaries. Furthermore, the XCQ4 approach provides better distributions of stress near the crack tip, which is rarely obtained by the standard Q4 elements. This is a promising method for further application to other complex engineering problems.

The example with hard inclusions shows that the mechanical properties have become better when mixing hard particles compared with homogeneous materials and highlights the outstanding advantages of composites. In contrast, the fracture behavior of the plate with voids near the crack is worse. For both cases of discontinuity, K_I increases with the increase in crack length. The crack propagation simulation is also conducted. Different crack path predictions show the influence of the type of loads and the location of defects on the crack propagation path. The analysis provides valuable insights into predicting the structural strength of materials when designing structures containing different types of discontinuities.

Credit authorship contribution statement. Binh Hai Hoang: Methodology, Investigation, Manuscript editor. Vay Siu Lo and Bang Kim Tran: Gathering data, Checking the results, Manuscript review. Thien Tich Truong: Supervisor, Funding acquisition.

Declaration of competing interest. The authors declare that they have no known competing financial interests or personal relationships that could have appeared to influence the work reported in this paper.

REFERENCES

1. Belytschko T. and Black T. - Elastic crack growth in finite elements with minimal remeshing, Int. J. Numer. Methods Eng. **45** (1999) 601-620. https://doi.org/10.1002/(SICI)1097-0207(19990620)45:5<601::AID-NME598>3.0.CO;2-S

2. Moës N., Dolbow J. and Belytschko T. - A finite element method for crack growth without remeshing, Int. J. Numer. Methods Eng. **46** (1999) 131-150. https://doi.org/10.1002/(SICI)1097-0207(19990910)46:1<131::AID-NME726>3.0.CO;2-J

3. Nagashima T., Omoto Y., Tani S. - Stress intensity factor analysis of interface cracks using X-FEM, Int. J. Numer. Mech. Eng. **28** (2003) 1151-1173. https://doi.org/10.1002/nme.604

4. Sukumar N., Huang Z. Y., Prévost J. –H., Suo Z. - Partition of unity enrichment for bimaterial interface cracks, Int. J. Numer. Mech. Eng. **59** (2004) 1075-1102. https://doi.org/10.1002/nme.902

5. Wang Y., Waisman H. - Material-dependent crack-tip enrichment functions in XFEM for modeling interfacial cracks in bimaterials, Int. J. Numer. Mech. Eng. **112** (2017) 1495-1518. https://doi.org/10.1002/nme.5566

6. Bui T. Q., Vo D. Q., Zhang C., Nguyen D. D. - A consecutive-interpolation quadrilateral element (CQ4): Formulation and applications, Finite Elem. Anal. Des. **84** (2014) 14-31. https://doi.org/10.1016/j.finel.2014.02.004

7. Zheng C., Wu S. C., Tang X. H., Zhang J. H. - A novel twice-interpolation finite element method for solid mechanics problems, Acta Mech. Sin. **26** (2010) 265-278. https://doi.org/10.1007/s10409-009-0265-3

8. Wu S. C., Zhang W. H., Peng X., Miao B. R. - A twice-interpolation finite element method (TFEM) for crack propagation problems, Int. J. Comput. Methods **9** (2012) https://doi.org/10.1142/S0219876212500557

9. Nguyen N. H., Nguyen K. C., Nguyen D. K., Nguyen X. H., Abdel-Wahab M. - A consecutive-interpolation polyhedral finite element method for solid structures, Int. J. Numer. Methods Eng. **122** (2021) 5692-5717. https://doi.org/10.1002/nme.6769

10. Nguyen N. H., Nguyen X. H., Abdel-Wahab M. - Dynamic Analysis of 3D Solid Structure Using a Consecutive-Interpolation Over Polyhedral Element Mesh, Proceedings of the 4th International Conference on Numerical Modelling in Engineering (2022) 1-8. https://doi.org/10.1007/978-981-16-8806-5_1

11. Nguyen N. H., Le C. T., Nguyen D. K., Nguyen X. H., Abdel-Wahab M. - Three-dimensional polyhedral finite element method for the analysis of multi-directional functionally graded solid shells, Compos. Struct. **305** (2023) 116538. https://doi.org/10.1016/j.compstruct.2022.116538

12. Kang Z., Bui T. Q., Nguyen D. D., Saitoh T., Hirose S. - An extended consecutive-interpolation quadrilateral element (XCQ4) applied to linear elastic fracture mechanics, Acta Mech. **226** (2015) 3991-4015. https://doi.org/10.1007/s00707-015-1451-y

13. Kang Z., Bui T. Q., Saitoh T., Hirose S. - Quasi-static crack propagation simulation by an enhanced nodal gradient finite element with different enrichments, Theor. Appl. Fract. Mech. **87** (2017) 61-77. https://doi.org/10.1016/j.tafmec.2016.10.006

14. Truong T. T., Tran B. K., Lo V. S., Nguyen N. T., Nguyen M. N. - Bimaterial interface crack analysis using an extended consecutive-interpolation quadrilateral element, Vietnam J. Sci. Technol. **60** (2022) 869-881. https://doi.org/10.15625/2525-2518/16172

15. Mohammadi S. - XFEM Fracture Analysis of Composites, XFEM Fracture Analysis of Composites (2012). https://doi.org/10.1002/9781118443378

16. An X., Ma G., Cai Y., Zhu H. - A new way to treat material discontinuities in the numerical manifold method, Comput. Methods Appl. Mech. Eng. **200** (2011) 3296-3308. https://doi.org/10.1016/J.CMA.2011.08.004

17. Nguyen H. D., Huang S-C. - Use of XTFEM based on the consecutive interpolation procedure of quadrilateral element to calculate J-integral and SIFs of an FGM plate, Theor. Appl. Fract. Mech. **127** (2023) 103985. https://doi.org/10.1016/j.tafmec.2023.103985

18. Lal A., Vaghela B. M., Mishra K. - Numerical Analysis of an Edge Crack Isotropic Plate with Void/Inclusions under Different Loading by Implementing XFEM, J. Appl. Comput. Mech. **7** (2021) 1362-1382. https://doi.org/10.22055/jacm.2019.31268.1848

19. Moës N., Cloirec M., Cartraud P., Remacle J.-F. - A computational approach to handle complex microstructure geometries, Comput. Methods Appl. Mech. Eng. **192** (2003) 3163-3177. https://doi.org/10.1016/S0045-7825(03)00346-3

20. Yang Y., Xu D., Sun G., Zheng H. - Modeling complex crack problems using the three-node triangular element fitted to numerical manifold method with continuous nodal stress, Sci. China Technol. Sci. **60** (2017) 1537-1547. https://doi.org/10.1007/s11431-016-0733-4

21. Nguyen M. N., Bui T. Q., Truong T. T., Tanaka S., Hirose S. - Numerical analysis of 3-D solids and composite structures by an enhanced 8-node hexahedral element, Finite Elem. Anal. Des. **131** (2017) 1-16. https://doi.org/10.1016/j.finel.2017.04.002

22. Nguyen T. N. , Bui Q. T., Nguyen N. M., Truong T. T. - Meshfree thermomechanical crack growth simulations with new numerical integration scheme. Eng. Fract. Mech. **235** (2020) 107121. https://doi.org/10.1016/j.engfracmech.2020.107121

23. Ventura G., Budyn E., Belytschko T. - Vector level sets for description of propagating cracks in finite elements. Int. J. Numer. Methods Eng. **58** (2003) 1571-1592. https://doi.org/10.1002/nme.829

24. Limtrakarn W., Dechaumphai P. - Adaptive finite element method to determine KI and KII of crack plate with different Einclusion/Eplate ratio, Trans. Can. Soc. Mech. Eng. **35** (2011) 355-368. https://doi.org/10.1139/tcsme-2011-0020

25. Ewalds H. and Wanhill R. - Fracture Mechanics, Edward Arnold, New York, 1989.